Draft version February 5, 2008
Preprint typeset using LaTeX style emulateapj

HIGH-RESOLUTION OPTICAL ROTATION CURVES OF LOW-LUMINOSITY SPIRAL GALAXIES

L. D. Matthews[1]
J. S. Gallagher, III[2]

Draft version February 5, 2008

ABSTRACT

We present optical longslit spectroscopic observations of 21 low-luminosity, extreme late-type spiral galaxies. Our sample is comprised of Sc-Sm Local Supercluster spirals with moderate-to-low optical surface brightnesses and with luminosities at the low end for spiral disk galaxies ($M_V \geq -18.8$). For each galaxy we have measured high spatial resolution position-velocity (P-V) curves using the Hα emission line, and for 15 of the galaxies we also derive major axis rotation curves. In $\sim$50% of our sample, the P-V curves show significant asymmetries in shape, extent, and/or amplitude on the approaching and receding sides of the disk. A number of the P-V curves are still rising to the last measured point, or reach a clear turnover on only one side. In most instances we find good agreement between the kinematic centers of extreme late-type spirals as defined by the global H I emission profile and by their optical continuum, although in a few cases we see evidence of possible real offsets. In spite of their shallow central gravitational potentials, at least 6 of the galaxies in our sample possess semi-stellar nuclei that appear to be compact nuclear star clusters; in 5 of these cases we see kinematic signatures in the P-V curves at the location of the nucleus. Finally, we find that like giant spirals, our sample galaxies have higher specific angular momenta than predicted by current cold dark matter models.

Subject headings: galaxies: general—galaxies: spiral—galaxies: kinematics and dynamics—galaxies: fundamental parameters

1. INTRODUCTION

1.1. *Background*

Matthews & Gallagher (1997; hereafter MG97) used the term "extreme late-type spirals" to refer to the lowest-luminosity rotationally-supported disk galaxies that still exhibit regular disk structure and well-defined optical centers. Typically these are moderate-to-low surface brightness Sc-Sm spirals that represent the low-end extremes of properties such as mass, luminosity, and size for a given Hubble type.

Extreme late-type spirals are among the dynamically simplest of disk galaxies: they tend to be pure disk systems, often with weak or absent spiral arm structure. Some extreme late-type spirals also appear to have undergone only minimal dynamical heating (e.g., Matthews 2000). However, in spite of their apparent simplicity, there is evidence of a variety of intriguing structural and dynamical phenomena in these small galaxies, including: multi-component disk structure (Matthews 2000); kinematically lopsided disks (e.g., Matthews, van Driel, & Gallagher 1998; Swaters et al. 1999; Matthews & Uson 2002); and compact starcluster nuclei (e.g., Matthews et al. 1999; Böker et al. 2001,2002). High-quality kinematic information for extreme late-type spirals is clearly desirable in order to further explore these trends.

Recently, the acquisition of kinematic information, particularly disk rotation curves, for low-luminosity and low surface brightness (LSB) spirals has also become of considerable interest for exploring broader issues relevant to our overall understanding of galaxy formation and the nature of galaxian dark matter. From numerous studies, it has now been found that the dynamics of these types of galaxies often appear to be dominated by dark matter even at very small galactocentric radii (e.g., Jobin & Carignan 1990; Côté, Carignan, & Sancisi 1991; Martimbeau, Carignan, & Roy 1994; Meurer et al. 1996; McGaugh & de Blok 1998; de Blok et al. 2001). Because the contribution to the overall dynamics from the visible matter in these faint disk systems is consequently quite small, this means that extreme late-type/LSB spirals can provide us with some of the most stringent constraints on dark matter halo properties of galaxies, and may hold a key to testing important classes of galaxy formation paradigms and cosmological models (e.g., Kravtsov et al. 1998; van den Bosch et al. 2000; Iliev & Shapiro 2001; van den Bosch, Burkert, & Swaters 2001).

Until recently, most of the rotation curves that have been obtained for extreme late-type spirals, especially LSB systems, were derived from H I aperture synthesis observations (e.g., Carignan, Sancisi, & van Albada 1988; Bosma, van der Hulst, & Athanassoula 1988; van der Hulst et al. 1993; de Blok, McGaugh, & van der Hulst 1996; Swaters 1999). Unfortunately, many of the H I rotation curves available for extreme late-type spirals suffer from poor angular resolution, leading in some cases to significant beam smearing, whereby the slope of the inner, rising portion of the rotation curve is underestimated (see Swaters 1999;

[1]Harvard-Smithsonian Center for Astrophysics, 60 Garden Street, MS-42, Cambridge, MA 02138 USA; Electronic mail: lmatthew@cfa.harvard.edu
[2]Department of Astronomy, University of Wisconsin-Madison, 475 N. Charter Street, Madison, WI 53706 USA

Swaters, Madore, & Trewhella 2000; van den Bosch et al. 2000). This in turn hampers attempts to perform accurate rotation curve mass decompositions and to meaningfully constrain the shape of the dark matter halo (e.g., Blais-Ouellette et al. 1999; van den Bosch et al. 2000). Beam smearing can be particularly problematic for the extreme late-type spirals, since these systems are physically small, and at distances of 10-20 Mpc, have angular sizes of only a few arcminutes or less. For this reason, *optical* kinematic data (i.e., longslit emission line spectroscopy or Fabry-Perot interferometry), which have higher spatial and spectral resolution, offer a more accurate means to map the inner rotation curve of extreme late-type spirals. These observations can thus serve as an extremely valuable complement to H I observations in mapping the full disk rotation curves (e.g., de Blok et al. 2001). The combination of optical and H I data is also powerful for constraining disk angular momenta (e.g., van den Bosch et al. 2001; see also Section **??**) and for comparing the kinematics of the ionized versus the neutral gas. Finally, high-resolution optical kinematic data provide unique information in their own right, such as kinematically confirming the presence of compact star cluster nuclei in small spirals (see Section 5.3).

1.2. *The Present Study*

MG97 presented optical B and V CCD photometry for a sample of 49 extreme late-type spiral galaxies with $\delta < -18^\circ$. Their sample consisted of Sc-Sm field spirals, all within the Local Supercluster (V_h $\leq$3000 km s^{-1}.). Although these objects are of relatively low luminosity and span a variety of morphological types (see Figure 11 of MG97), all have regular disk structures and well-defined optical centers, distinguishing them structurally from dwarf irregular (dIrr) galaxies of similar luminosities. Most, but not all of the galaxies are objects of low mean optical surface brightness ($\bar{\mu}_{V,i} \gtrsim$23 mag arcsec^{-2}). Generally these galaxies are H I-rich, with high $\mathcal{M}_{HI}/L_B$ ratios for their Hubble types (MG97; Matthews, van Driel, & Gallagher 1998). Finally, all of the galaxies in the MG97 sample exhibit significant rotational broadening in their global H I profiles, with all but few objects showing double-peaked H I spectra (Fouqué et al. 1990; Matthews et al. 1998).

In this paper we use optical longslit emission line (Hα) spectroscopy to explore the rotational properties of 21 of the MG97 galaxies. In Section **??** we describe our sample selection. In Section **??** & **??** we describe our observations and data reduction, respectively. We present position-velocity (P-V) diagrams derived from the new Hα data in Section **??**, and compare them to the global H I profiles of the galaxies. For the 15 galaxies with highest-quality optical data, we also derive major axis rotation curves. We discuss characteristics of our P-V plots and rotation curves further in Section **??**, including the presence of kinematic asymmetries (Section 5.2.2). In Section 5.3, we investigate the dynamical signatures of the semi-stellar nuclei on the rotation curves of several of the galaxies and use these to derive crude mass estimates for the nuclei, while in Section **??** we briefly comment on the specific angular momenta of the disks in our sample. Finally, in the Appendix we provide comments on our individual longslit spectra.

Our optical disk rotation profiles are measured using the Hα emission line, which is in general only easily observable to within $r \lesssim D_{25}$ in most normal, bright galaxies, and to only a fraction of D_{25} in faint, extreme late-type systems (e.g., Table 2). Therefore, ultimately the observations we present should be combined with extended H I rotation curves to gauge the full disk rotation of our sample galaxies. Currently H I rotation curve data are not available for the bulk of the galaxies in our sample, hence it is intended that the results presented here will provide an aid for selecting objects suitable for future H I mapping. For this reason, we are also making available in electronic format all of our measured P-V data (Table 3).

2. SAMPLE SELECTION

For our spectroscopic measurements we selected from MG97 twenty-one extreme late-type spiral galaxies covering a range of optical morphologies. Where possible, preference was given to galaxies with moderate-to-high inclinations. All of our targets have radial velocities V_h <2800 km s^{-1} and therefore reasonable spatial resolution for these systems can be achieved from the ground under average seeing conditions. Some global properties of our targets are given in Tables 1 & 2. Sample broadband images of 4 of the galaxies are shown in Figure 1.

3. OBSERVATIONS

Our longslit spectroscopic observations were obtained during two nights in 1995 January using the 4-m telescope and Ritchey-Chrétien (R-C) Spectrograph at the Cerro Tololo Inter-American Observatory (CTIO)[3]. All spectra were taken under clear conditions. Seeing throughout the run was $\sim$0$''$.8-1$''$.0.

Our R-C spectrograph set-up included the folded Schmidt camera at the f/7.8 focus. The detector was a Tek 1024×1024 CCD with Arcon controller. With the Arcon controller, the CCD is divided into four quadrants, each with its own amplifier. This results in a slightly different gain and readnoise for each of the four sections of the chip. The mean gain was 1.25 e^-/ADU and the mean readnoise was 4.3 e^- rms. At the f/7.8 focus, the folded Schmidt camera yielded a plate scale of 0$''$.8 per 24μm pixel on the Tek CCD. Our slit length and width were 328$''$ and 1$''$.5, respectively. We used filter GG495 with grating KPGLG, which has 860 l/mm, a blaze of 11000Å at first order. This yielded a dispersion of 0.68Å per pixel and spectral coverage $\Delta\lambda$ of roughly 615Å centered on the redshifted Hα $\lambda\lambda$6562.82Å line. This $\Delta\lambda$ interval also includes the [N II] λ6583.41Å, and [S II] $\lambda\lambda$6718.26,6732.64Å emission lines.

Using position angles from the literature or estimated from previously obtained CCD images, we generally strove to place the spectrograph slit along the major axis of each target (or in two cases, along the galaxy bar; see Table 1). Unfortunately, in a few cases, less optimal slit position angles were achieved (see Table 1 and the Appendix). Hereafter we denote the offset in angle between the photometric major axis and the observed slit position angle as $\Delta\phi$. All

[3]Cerro Tololo Inter-American Observatory is operated by the Association of Universities for Research, Inc. under contract with the National Science Foundation

of our target galaxies have small enough optical angular sizes such that they were fully sampled with the 328″ slit length.

Our exposure times for each target ranged from 500-2000s (see Table 1). Whenever possible, two independent exposures were obtained to aid in cosmic ray rejection. During each observation, a ThAr comparison lamp exposure was also acquired at the same telescope position as the target galaxy for use in correction for geometric distortions (see below).

4. DATA REDUCTION

Our data were reduced using the standard spectral reduction and analysis packages available in *IRAF*[4]. Overscan corrections were applied to each frame using the QUADPROC routine. Sequences of bias frames taken each afternoon showed the bias level of the Tek CCD to be extremely unstable. Count levels in the bias images ranged from 3 to 8 ADU, but the underlying structure varied widely for frames obtained only minutes apart. In addition, a ripple pattern with an amplitude ∼0.5 ADU was visible in most bias frames, and this pattern was found to shift in location from one bias frame to another. For this reason, we were not able to reliably subtract the bias level from our images. Since the count levels in the bias can be significant relative to some of the faint emission line signals from our targets, we were unable to obtain accurate absolute line fluxes or line ratios from the present data. This also introduces an additional source of error in determining the centroid of the galaxy in cases where the galaxy continuum is fairly weak (see below). However, our absolute wavelength calibration should not be affected.

The *IRAF* BACKGROUND task was used to remove scattered light from our images, and the data were flatfielded using normalized domeflats. The task ILLUM was then used to apply an illumination correction derived from twilight sky exposures. This procedure yielded images that were flat to a fraction of a per cent. A sample of one of our flatfielded spectra is shown in Figure 2.

Cosmic rays were identified by blinking the multiple object exposures when available, otherwise by visual inspection. In cases where two object exposures were available, cosmic ray events in the vicinity of galaxian emission features were removed by replacing the affected pixels with the corresponding pixel values from the other image. When only one exposure was available, cosmic rays were removed by interpolating from the surrounding pixels (in cases where they landed on background regions), or by simply masking the affected pixel(s) (in instances where they were superimposed on an emission line).

To derive a correction for geometric distortions, we utilized our ThAr comparison spectra and followed a procedure similar to that outlined by Massey, Valdes, & Barnes (1992). We identified the lines in the ThAr lamp spectra, and then applied to our galaxy spectra the geometric transformation of λ as a function of the position on the CCD by fitting a sixth order, two-dimensional Chebyshev function using the task FITCOORDS. Based on the dispersion solutions found by FITCOORDS, we transformed all rows along our object spectra to identical linear wavelength scales using the task TRANSFORM, which performed the necessary interpolations using a third order spline function. The rms residuals for the wavelength solutions were typically 0.05 pixel, corresponding to 0.034 Å (∼1.6 km s^{-1} at Hα). As a check, we also attempted the corrections for geometric distortions using lines identified from night sky spectra. We found the results of the two approaches to be indistinguishable. Aside from the expected flexure shifts (which affect absolute, but not relative wavelength calibrations; see below), we found our dispersion solutions to be very stable over the course of the run.

During our reductions we found the multiple standard star exposures obtained for the purpose of correcting the tilt of the spatial axis relative to the edge of the detector to be inadequate to map the trace along the full extent of the slit, hence we were unable to properly correct for this effect. The tilt is approximately 2 pixels across the full 1024-pixel width of the CCD. This does not affect our absolute wavelength calibration, but means that when a spectrum is extracted parallel to the edge of the CCD, the Hα, [N II], and [S II] emission lines will all sample slightly different parts of the galaxy rotation curve. This effect matters little for our purposes, since the [N II] and [S II] emission lines were often quite weak in our galaxies and were generally not useful for mapping the galaxy rotation curve over significant angular extents. In addition, these lines were frequently too noisy to provide a reliable check on the radial velocitues derived from the Hα features.

To derive P-V curves for our galaxies, we used the *IRAF* APALL task to extract a series of spectra along the slit for each object. Because most of the galaxies have at least some degree of asymmetry, and because many of the rotation profiles are rising to the last measured point, we were unable to use a point of symmetry to determine the systemic velocity. However, all of the galaxies had sufficient continuum emission such that the peak of the continuum could be used for the determination of the galaxy center. Galaxy centroid determination was therefore accomplished by plotting the average of 10 columns on either side of the galaxy Hα emission, and adopting as the center the position of the peak value of the continuum. We estimate this method yields a galaxy center good to roughly one-third of a pixel (i.e. ∼10 km s^{-1}), accounting for the bias level uncertainties described above.

We measured the spatial profile width of a standard star to be roughly 10 pixels, and adopted this as our extraction aperture width. For each extraction, the Hα line's centroid was determined by averaging anywhere between 8 and 19 dispersion lines, depending on the emission line strength and velocity dispersion in a given object. A series of extraction apertures was then placed by hand along the full extent of the slit, with roughly 3 pixels overlap between consecutive apertures. Background regions for each aperture were set interactively, and subtracted by fitting a second order Chebyshev function over the region.

A by-product of the APALL task for each extracted object spectrum is the spectrum of the subtracted sky background, which contains numerous OH night sky lines. Because of our moderately long exposures, these lines were of high signal-to-noise. Osterbrock et al. (1996) compiled an accurate list of reference wavelengths for these lines, thus

[4]IRAF is distributed by the National Optical Astronomy Observatories, which is operated by the Associated Universities for Research in Astronomy, Inc., under cooperative agreement with the National Science Foundation.

we were able to utilize them to obtain a final dispersion solution for our spectra. Use of this wavelength calibration technique eliminates the need to separately correct the zero-point solution for the effects of spectrograph flexure.

As a final step, we measured the wavelengths of the emission lines in the extracted spectra using SPLOT to perform Gaussian fits to the line profiles. The resulting wavelengths at each point were converted to radial velocities and corrected for heliocentric motion. The uncertainties in each data point ($\pm\sigma_V$) were computed as $\sigma_V = RS^{-0.5}$ km s^{-1}, where R is the velocity resolution per pixel and S is the mean signal-to-noise ratio of the three brightest pixels in each line profile. The sizes of the error bars plotted on Figure 4 (discussed below) thus give an indication of the relative strength of the Hα line in our various target galaxies.

5. RESULTS

5.1. *Optical Versus Radio Systemic Velocities*

Figure 3 shows a plot comparing the heliocentric radial velocities derived from our new optical rotation curves with the values derived from global H I spectra by Fouqué et al. (1990) and Matthews et al. (1998). Overall the agreement is excellent. This agreement suggests that most extreme late-type spirals seem to have well-defined centers in spite of their often diffuse stellar disks and shallow central potentials. Consequently, this can offer an additional means of distinguishing extreme late-type spirals from true irregular galaxies.

In our sample we have only 6 instances where we see a discrepancy of more than $\sim$10 km s^{-1} between the radial velocities derived from optical versus radio measurements. Because of the small formal measurement errors on both the optical and H I radial velocities ($\lesssim$10 km s^{-1} and $\lesssim$5 km s^{-1}, respectively), it is possible that in at least some of these cases, these discrepencies may a consequence of true offsets between the centroid of the global H I profile and the center of the galaxy defined by the optical continuum. Similar offsets have been reported in other moderate-to-low-mass, late-type spirals (Colin & Athanassoula 1981; Minniti, Olszewski, & Reike 1993; Rownd, Dickey, & Helou 1994).

In 4 of the 6 galaxies where $V_{sys,opt}$ and $V_{sys,HI}$ differ by more than 10 km s^{-1}, asymmetries are observed in the global H I profiles (see Figure 4; Section 5.2.2). Together these two trends may hint that these could be galaxies where the stellar disk is in libration about the minimum of the H I or dark matter potential (Kornreich et al. 1998; see also Levine & Sparke 1998; Noordermeer, Sparke, & Levine 2001). Levine & Sparke (1998) and Noordermeer et al. (2001) have shown through numerical simulations and modelling that such configurations can reproduce the lopsidedness observed in many extreme late-type spirals (see also below). Nonetheless, as we discuss below, approximately one-third of our sample appears to exhibit kinematic lopsideness, hence in the majority of lopsided galaxies, the peak of the stellar density correlates surprisingly well with the centroid of the global H I profile.[5] The centroid of the global H I profile thus generally seems to be a good indicator of the location of the minimum of the disk potential, even in most asymmetric galaxies. This would seem to argue that the overall potential of the galaxies (established mainly by the dark matter halo in the small systems considered here) are symmetric on large scales, even in cases where asymmetries in the visible matter or velocity field are observed (cf. Rix & Zaritsky 1995; Jog 1999).

5.2. *Position-Velocity Plots and Rotation Curves*

The position-velocity (P-V) curves derived from our final spectra are presented in Figure 4. When available, we plot next to the Hα P-V curves the corresponding high resolution global H I spectra from Matthews et al. (1998). Parameters measured from the optical data, including systemic velocities and the peak measured rotational velocities, are presented in Table 2 along with photometric and global H I parameters from the literature.

From Figure 4 and Table 2 it can be seen that among the galaxies where $|\Delta\phi| < 30°$ (i.e., cases where the galaxy's major axis and the spectrograph slit were well-aligned), the disk rotation velocities measured in the plane of the sky from our new optical data ($\Delta V_{H\alpha}$) agree to within measurement errors with those derived from global H I data (W_{20}) about half of the time. In the remaining cases, H II regions were not observable to sufficiently large radii to reach the peak of the rotation curves in our longslit measurements of these optically faint galaxies.

For the 15 galaxies in our sample with $i \geq 40°$ and $|\Delta\phi| < 30°$, we derived deprojected rotation curves along the disk major axis (Figure 5). The disks were assumed to be in circular rotation, and the measured heliocentric radial velocities at each point were projected onto the plane of the galaxy using the relations given by Rubin, Ford, & Thonnard (1980) to correct for disk inclination and small position angle misalignments. In cases where the systemic velocities derived from global H I spectra differed from our new optically derived values, we used whichever value minimized the asymmetry of the folded rotation curve. Distances for the galaxies were adopted from MG97.

5.2.1. *The Shapes of Extreme Late-Type Spiral Rotation Profiles*

We see from Figures 4 & 5 that most of our sample galaxies show a leisurely rise in rotational velocity with increasing radius, and many have rotation profiles that continue to rise to the last measured point. Similar rotation curve shapes are frequently seen among the extreme late-type spiral rotation curves measured by other workers using the Hα emission line (e.g., Goad & Roberts 1981; Karachentsev 1991; Makarov, Burenkov, & Tyurina 1999; Swaters 1999; Dalcanton & Bernstein 2000; McGaugh, Rubin, & de Blok 2001) and have become well-established as the hallmark of small, dark matter-dominated disk galaxies. These are in stark contrast to giant spirals, where rotation curves typically rise rapidly to V_{max} within the inner portion of the stellar disk (cf. Casertano & van Gorkom 1991).

In 3 of the most extreme cases (ESO 418-008; ESO 504-017; ESO 440-049), we can partially attribute the shallow

[5]The H I systemic velocity we refer to is defined as the midpoint of the global profile measured at a level equal to either 20% or 50% of the peak flux density (Fouqué et al. 1990; Matthews et al. 1998).

velocity gradients in our observed P-V plots to position angle misalignments between the spectrograph slit and the galaxy major axis ($|\Delta\phi| > 30°$; see Table 1). However, in all other instances, the slow rise of the rotation velocity as a function of r appears to be real, and thus be indicative of low matter densities within the inner disks of these galaxies. For example, ESO 358-060 has a particularly shallow rotation curve in spite of being nearly edge-on (i=85°). This galaxy has a very low deprojected central surface brightness [$\mu_V(0) \approx$25.5 mag arcsec^{-2}] and would likely be nearly invisible if seen close to face-on in an optical broadband survey image. As demonstrated by Matthews & Wood (2001), such a shallow rotation curve cannot be explained solely by projection effects or internal extinction, even in edge-on systems.

In only a few of our sample galaxies do we see a clear turnover or flattening of the optical P-V curve on both the approaching and receding sides: ESO 482-005, ESO 504-025, ESO 440-049, ESO 443-079. These galaxies are some of the "earlier" Hubble type objects in our sample (Sc-Sd), and include some of the sample galaxies with the most clearly-defined spiral structure. In some other cases, we see an apparent turnover on only one side of the P-V curve (ESO358-020; ESO 425-008; ESO 438-005; ESO 380-025; ESO 508-034; ESO 444-033; see also Section 5.2.2).

We find that even in instances where a turnover or flattening is seen, our observed P-V curves rarely extend significantly beyond this turnover. Moreover, while the Sc-Scd galaxies in our sample seem more prone to exhibiting flattening of their P-V curves, we otherwise see no absolute correlation between Hubble type, galaxy morphology, or luminosity and the P-V or rotation curve shape in our sample. For example, ESO 504-025 and ESO 358-020 both have $M_V \sim$-17.5 and $i \sim 40°$, but have very different inner rotation curve shapes and amplitudes. At the same time, we also see cases where optically rather dissimilar galaxies (e.g., ESO 380-025 and ESO 508-034) have similar rotation curve shapes and amplitudes. These rotation curves signatures may hold important clues as to the evolutionary histories of these galaxies—for example, the possibility that morphological tranformations may occur in late-type disk galaxies as a result of viscous evolution, interactions, or tidally-induced starbursts (e.g., Gallagher & Matthews 2001; Noguchi 2001; Matthews & Uson 2002).

Rotation curves that do not flatten within the optical galaxy imply that the bulk of the stellar disk is in solid body rotation. It has long been known that such rotation curves are common in gas-rich dIrr galaxies (e.g., Carignan & Freeman 1988; Carignan & Puche 1990; Côté et al. 1991; Casertano & van Gorkom 1991; Côté, Carignan, & Freeman 2000). However, while most such galaxies are still predominantly rotationally supported, many of the dIrrs with apparent solid-body rotation curves also have single-peaked global H I spectra, implying that solid body rotation persists to the outermost observable regions of the gas disk (e.g., Skillman 1996). In contrast, most of the galaxies in our sample have *double-peaked* global H I profiles (Figure 4; see also Fouqué et al. 1990; Matthews et al. 1998), which in turn implies that the outer rotation curve contains a flat or relatively flat region (cf. Giovanelli & Haynes 1988), although it may lie outside the stellar disk. H I data will clearly be needed to trace this portion of the disk rotation profiles in our present sample.

5.2.2. *Kinematic Asymmetries in Extreme Late-Type Spirals*

It is evident from Figures 4 & 5 that asymmetries are the rule rather than the exception for our extreme late-type spiral rotation profiles. Many of the P-V plots and rotation curves show significant differences in their radial extents on the approaching and receding sides. Often, the amplitudes of the two sides of the rotation curves also differ (sometimes by tens of kilometers per second), and in some cases, the rotation curves show differing velocity gradients on the two sides of the galaxy. Although there is frequently some uncertainty in defining the center of any given rotation curve, our sample nonetheless appears to contain some galaxies where the velocity differences between the approaching and receding sides are greater than 20%, in contrast to Swaters et al. (1999), who suggested that perhaps such significant (kinematic) asymmetries may not exist.

Based on statistical studies of high-quality global H I data, Richter & Sancisi (1994) and Haynes et al. (1998) found that H I profile asymmetries occur in approximately 50% of normal spirals. Matthews et al. (1998) explored the frequency of H I profile asymmetries in extreme late-type spirals and found that the frequency of lopsidedness may be even higher among small late-type spirals than among giant galaxies. Unfortunately, from asymmetries in the global H I profiles alone, it is not possible to assess whether these asymmetries arise from asymmetric gas distributions (e.g. as a result of accretion events; Rix & Zaritsky 1995; Zaritsky & Rix 1997) or from true kinematic lopsidedness, which in turn may indicate lopsidedness in the overall galaxy potential (e.g., Schoenmakers, Franx, & de Zeeuw 1997; Levine & Sparke 1998; Jog 1999). Our new optical spectra allow us to obtain additional insight into this question.

Six of the 17 galaxies in the present sample for which Matthews et al. (1998) obtained high precision global H I profiles were catagorized by Matthews et al. as having strong H I asymmetries (ESO 358-020, ESO 422-005; ESO 502-016; ESO 504-017; ESO 380-025; ESO 444-033). In 5 out of 6 of these cases, we find the optical rotation curve to have a greater amplitude on the same side as the H I "excess" in the global H I profile. Several of these cases also exhibit different velocity gradients on the approaching and receding sides of the disk. This latter effect is particularly pronounced in ESO 422-005 and ESO 444-033. This suggests that these asymmetries result from true lopsidedness in the disk kinematics rather than non-symmetric matter densities (see Swaters et al. 1999; Noordermeer et al. 2001). Among the 11 remaining galaxies in our sample whose H I profiles were analyzed by Matthews et al. and not classified as strongly asymmetric, we see a significant rotation curve *amplitude* asymmetry in only one other case (ESO 358-015), and a significant difference in the rates at which the two sides of the rotation curve rise in only ESO 358-015 and ESO 359-029. Strong asymmetries in the global H I profiles therefore appear to be good, although not perfect, predictors of lopsidedness in the disk kinematics. As noted above, we see additional galaxies in our sample whose rotation curves show asymmetries in terms of their *extents* on the two sides of the disk (e.g., ESO 305-009, ESO 425-008, ESO 438-005). However, in

these latter cases, it is possible that these asymmetries arise from asymmetric matter distributions as opposed to true lopsided kinematics.

We conclude that the results from our small sample are consistent with at least one-third of extreme late-type spirals exhibiting true kinematic asymmetries (see also Swaters et al. 1999), and hence possibly asymmetries in their overall potentials (but see Section 5.1) and with approximately 50% of extreme late-type spirals exhibiting either kinematic *or* structural asymmetries. Since all of the objects in our sample are field spirals, generally lying on the peripheries of loose groups or associations (Gallagher, Littleton, & Matthews 1995), it would seem unlikely that the lopsided natures of all of our sample galaxies are exclusively the result of very recent interactions with other galaxies, although there may be some exceptions (e.g., Matthews & Uson 2002).

Although asymmetries are common among disk galaxies covering a wide range of masses and luminosities (e.g., Baldwin, Lynden-Bell, & Sancisi 1980; Richter & Sancisi 1994; Haynes et al. 1998), our new data, and the findings of Matthews et al. (1998), hint that they are equally, or perhaps more common in low-mass spirals. Indeed, based on the models of Noordermeer et al. (2001), pronounced asymmetries are more persistent in galaxy systems where the dark matter halo strongly dominates the potential, as is expected in typical extreme late-type spirals (see also Levine & Sparke 1998). Using models with a disk lying off-center in a dark halo, Noordermeer et al. produced model rotation curves whose shapes were very similar to some of those seen in the present sample, i.e., showing differing slopes on the approaching and receding sides, and flattening of the rotation profile on one side only. Swaters et al. (1999) noted similar signatures in the rotation curves of the two asymmetric extreme late-type spirals that they analyzed.

5.3. *Kinematic Signatures of Semi-Stellar Nuclei in Extreme Late-Type Spirals*

Five of the extreme late-type spirals in the present sample were noted by MG97 to possess a compact, semi-stellar nucleus (ESO 359-029; ESO 358-015; ESO 305-009; ESO 504-025; ESO 505-013; see also Figure 1). The nucleus of ESO 359-029 was subsequently observed with the Planetary Camera 2 on the *Hubble Space Telescope* and demonstrated by Matthews et al. (1999) to be a true compact star cluster nucleus analogous to those at the centers of many brighter galaxies. Subsequently, one additional galaxy in our sample (ESO 418-008) has also been found to possess a compact star cluster nucleus based on *HST* imaging (Böker et al. 2002; Windhorst et al. 2002). Although the formation mechanism for these compact nuclei at the centers of such diffuse galaxies with shallow central potentials remains a mystery, these types of "naked" nuclei are now known to be commonplace at the centers of late-type, pure disk spirals (see also van den Bergh 1995; Phillips et al. 1996; Böker et al. 2001,2002).

In our present sample, in five of the cases where the presence of a compact nuclear feature is seen in the CCD images of MG97, we also see a signature of this nucleus in our spectroscopic data—i.e. the P-V curves exhibit reversals, breaks, or disturbances near the location of the nucleus (see Figure 4). This strongly suggests that in all of these cases, these nuclei are compact, massive star clusters rather than simply small nuclear H II regions.

If we assume that the ionized gas surrounding these nuclei is in Keplerian rotation, we can make very rough estimates of their masses from our present data—i.e., $M_{nuke} = V_{max,s}^2 r G^{-1}$, where G is the gravitational constant, r is the galactocentric distance along the major axis, and $V_{max,s}$ is the orbital semi-amplitude of the material orbiting the nucleus in the reference frame of the disk, after correction for inclination. Because the velocity and spatial resolution of our data are rather coarse relative to the amplitudes and spatial extents of these central rotation curve features, and because it is unclear whether the nuclear disk material will share the same inclination as the main disk of the galaxy, these calculations are necessarily very crude. Nonetheless, we estimate nuclear masses $M_{nuke} \sim 10^6 - 10^7\ \mathcal{M}_\odot$, comparable to the masses of low-luminosity star cluster nuclei derived for other late-type spirals [e.g., M33: $M_N \sim 2 \times 10^6\ \mathcal{M}_\odot$(Kormendy & McClure 1993); NGC 4449: $M_N > 4 \times 10^5\ \mathcal{M}_\odot$ (Böker et al. 2001); IC 342: $M_N \sim 6 \times 10^6\ \mathcal{M}_\odot$ (Böker, van der Marel, & Vacca 1999)].

As a final note, we draw attention to the fact that some of the nuclei in our present sample appear to be offset from the dynamical centers of the galaxies as defined by either the optical continuum and/or the centroid of the global H I profile (see also the Appendix). The frequent displacement of compact nuclei from the dynamical centers of galaxies has been discussed previously by Miller & Smith (1992; see also Levine & Sparke 1998) and may offer an important clue to the formation mechanism of the nuclei. Higher resolution spectroscopy of more extensive samples of these types of nuclei is clearly desirable in order to better understand their natures, to improve these mass estimates, and to help us understand their dynamical relationships to the surrounding disk material.

6. THE ANGULAR MOMENTUM OF SMALL DISK GALAXIES

In cold dark matter (CDM) galaxy formation models, protodisk baryons tend to efficiently lose angular momentum to their dark matter halos, resulting in a situation where the predicted sizes of galaxy disks are too compact by substantial factors (e.g., Navarro, Frenk, & White 1995; Navarro & Steinmetz 2000). Since our sample contains a variety of small disk galaxies, it provides an opportunity to constrain disk angular momenta at moderate galactic masses. These systems are of particular interest, since their moderate mass, yet gas-rich and relatively unevolved disks pose a challenge for proposed solutions to the angular momentum problem via internal evolution, such as intense star-forming events (cf. Efstathiou 2000; Silk 2001).

We calculated specific angular momenta j_D for the stellar disks in our present sample using the approximate disk scale lengths in MG97 and assuming $j_D \geq V_l/\alpha$, where the inverse exponential scale length is α and V_l is the peak of the linearly rising rotation curve. This is a lower bound, as the H I gas will have higher specific angular momentum, as will the stellar disks of galaxies where V_l is approached rapidly within 1-2 scale lengths. The result is that we find typical angular momenta of 100-200 km s^{-1} kpc for systems with $V_l \approx 100$ km s^{-1}. Thus this excercise reveals that our sample galaxies appear to fall on the normal an-

gular momentum-rotational velocity relationship found for giant spirals (e.g., Navarro & Steinmetz 2000) and that our data agree with results from H I rotation curve studies in showing that disks of gas-rich, moderate mass galaxies have normal specific angular momenta (see van den Bosch et al. 2001). Our findings therefore are consistent with the specific angular momenta of small, pure disk systems having been set during their formation (see Fall & Efstathiou 1980), in contradiction to the predictions of standard CDM models (cf. Navarro & Steinmetz 2000).

7. CONCLUSIONS

We have presented new optical longslit kinematic measurements for 21 low-luminosity, extreme late-type spiral galaxies using the Hα emission line. We have derived position-velocity (P-V) curves for all 21 galaxies, as well as deprojected major axis rotation curves for 15 of the objects. To facilitate future synthesis with H I rotation curve measurements, we have also made all of our P-V data available in electronic format.

Most of the extreme late-type spirals in our sample exhibit slowly rising, nearly linear P-V curves throughout a significant fraction of their stellar disks. Many of the P-V curves continue to rise to the last measured point in the optical galaxy, implying low central matter densities. The disks of these galaxies appear to follow the trend between specific angular momentum and rotational velocity seen in giant spirals, suggesting that the angular momenta of disks are not closely tied to the details of their structures or star formation histories, and are intrinsically larger than predicted by current cold dark matter models.

A significant fraction of our measured optical P-V curves are not symmetric, and our observations are consistent with $\sim$50% of extreme late-type spirals possessing kinematic and/or structural asymmetries. In some cases, this may also be manifested as an offset between the V_{sys} values measured from global H I spectra and that measured from the optical data, although in most cases those values show excellent agreement. We find that lopsided global H I profiles appear to be a good, although not a perfect predictor of kinematic asymmetries in extreme late-type spiral disks.

Five of the extreme late-type spirals in our sample possess compact, semi-stellar nuclei that produce kinematic signatures in the galaxy rotation curves. Rough mass estimates help to confirm that these are massive, highly compact star nuclei star clusters analogous to those seen in brighter galaxies. Such nuclei appear to be a common feature of extreme late-type spiral galaxies in spite of their apparently weak central gravitational potentials.

We are grateful to the late R. Schommer as well as the CTIO staff for their assistance with the RC Spectrograph observations. LDM completed a portion of this work while supported by a Clay Fellowship from the Harvard-Smithsonian Center for Astrophysics. JSG thanks the University of Wisconsin Graduate School and for their partial support of this research.

REFERENCES

Baldwin, J. E., Lynden-Bell, D., & Sancisi, R. 1980, MNRAS, 193, 313
Blais-Ouellette, S., Carignan, C., Amran, P., & Côté, S. 1999, AJ, 118, 2123
Böker, T., Laine, S., van der Marel, R. P., Sarzi, M., Rix, H.-W., Ho, L. C., & Shields, J. C. 2002, AJ, in press (astro-ph/0112086)
Böker, T., van der Marel, R. P., Mazzuca, L., Rix, H.-W., Rudnick, G., Ho, L. C., & Shields, J. C. 2001, AJ, 121, 1473
Böker, T., van der Marel, R. P., & Vacca, W. D. 1999, AJ, 118, 831
Bosma, A., van der Hulst, J. M., & Athanassoula, E. 1988, A&A, 198, 100
Carignan, C. & Freeman, K. C. 1988, ApJ, 347, 760
Carignan, C. & Puche, D. 1990, AJ, 100, 641
Carignan, C., Sancisi, R., & van Albada T. S. 1988, AJ, 95, 37
Casertano S. & van Gorkom J. H. 1991, AJ, 101, 1231
Colin, J. & Athanassoula, E. 1981, A&A, 97, 63
Côté, S., Carignan, C., & Sancisi, R. 1991, AJ, 102, 904
Côté, S., Carignan, C., & Freeman, K. C. 2000, AJ, 120, 3027
Dalcanton, J. J. & Bernstein, R. A. 2000, in Dynamics of Galaxies: from the Early Universe to the Present, ed. by F. Combes, G. A. Mamon, and V. Charmandaris, (San Franciso: ASP), 161
de Blok, W. J. G., McGaugh, S. S., Bosma, A., & Rubin, V. C. 2001, ApJ, 552, L23
de Blok, W. J. G., McGaugh, S. S., & van der Hulst, J. M. 1996, MNRAS, 283, 18
Efstathiou, G. 2000, MNRAS, 317, 697
Fall, S. M. & Efstathiou, G. 1980, MNRAS, 193, 189
Fouqué, P., Bottinelli, L., Durand, N., Gouguenheim, L., & Paturel, G. 1990, A&AS, 86, 473
Gallagher, J. S., Littleton, J. E., & Matthews, L. D. 1995, AJ, 109, 2003
Gallagher, J. S. & Matthews, L. D. 2001, in Modes of Star Formation and the Origin of Field Star Populations, ed. by E. Grebel & W. Brandner, (San Francisco: ASP), in press
Giovanelli, R., & Haynes, M. P. 1988, in Galactic and Extragalactic Radio Astronomy, edited by G. L. Verschuur and K. I. Kellermann (New York: Springer-Verlag), 526
Goad, J. W. & Roberts, M. S. 1981, ApJ, 250, 79
Haynes, M. P., van Zee, L., Hogg, D. E., Roberts, M. S., & Maddalena, R. J. 1998, AJ, 115, 62
Iliev, I. T., Shapiro, P. R. 2001, ApJ, 546, L5
Jobin, M. & Carignan, C. 1990, AJ, 100, 648
Jog, C. J. 1999, ApJ, 522, 661
Karachentsev, I. D. 1991, Sov. Astron. Let., 17, 206
Kormendy, J. & McClure, R. D. 1993, AJ, 105, 1793
Kornreich, D. A., Haynes, M. P., & Lovelace, R. V. E. 1998, AJ, 116, 2263
Kravtsov, A. V., Klypin, A. A, Bullock, J. S., & Primack, J. R. 1998, ApJ, 502, 48
Levine, S. E. & Sparke, L. S. 1998, ApJ, 496, L13
Martimbeau, N., Carignan, C., & Roy, J.-R. 1994, AJ, 107, 543
Makarov, D. I., Burenkov, A. N., & Tyurina, N. V. 1999, Astron. Let., 25, 706
Massey, P., Valdes, F., & Barnes, J. 1992, A User's Guide to Reducing Slit Spectra with IRAF (http://iraf.noao.edu/docs/spectra.html)
Matthews, L. D. 2000, AJ, 120, 1764
Matthews, L. D. et al. 1999, AJ, 118, 208
Matthews, L. D. & Gallagher, J. S. 1997, AJ, 114, 1899 (MG97)
Matthews, L. D. & Uson, J. M. 2002, in Seeing Through the Dust: The Detection of H I and the Exploration of the ISM in Galaxies, ed. by R. Taylor, T. Landecker, & T. Willis (San Francisco: ASP), in press
Matthews, L. D., van Driel, W., & Gallagher, J. S. 1998, AJ, 116, 1169
Matthews, L. D. & Wood, K. 2001, ApJ, 548, 150 2001
McGaugh, S. S. & de Blok, W. J. G. 1998, ApJ, 499, 41
McGaugh, S. S., Rubin, V. C., & de Blok, W. J. G. 2001, AJ, 122, 2381
Meurer, G. R., Carignan, C., Beaulieu, S. F., & Freeman, K. C. 1996, AJ, 111, 1551
Miller, R. H. & Smith, B. F. 1992, ApJ, 393, 508
Minniti, D., Olszewski, E. W., & Rieke, M. 1993, ApJ, 410, L79
Navarro, J. F., Frenk, C. S., & White, S. D. M. 1995, MNRAS, 275, 56
Navarro, J. F. & Steinmetz, M. 2000, ApJ, 538, 477
Noguchi, M. 2001, ApJ, 555, 289
Noordermeer, E., Sparke, L. S., & Levine, S. E. 2001, MNRAS, 328, 1064
Osterbrock, D. E., Fulbright, J. P., Martel, A. R., Keane, M. J., & Trager, S. C. 1996, PASP, 108, 277
Phillips, A. C., Illingworth, G. D., MacKenty, J. W., & Franx, M. 1996, AJ, 111, 1566
Richter, O.-G. & Sancisi, R. 1994, A&A, 290, 9
Rix, H.-W. & Zaritsky, D. 1995, ApJ, 447, 118

Rownd, B. K., Dickey, J. M., & Helou, G. 1994, AJ, 108, 1638
Rubin, V. C., Ford, W. K. Jr., & Thonnard, N. 1980, ApJ, 238, 471
Schoenmakers, R. H. M., Franx, M., & de Zeeuw, P. T. 1997, MNRAS, 292, 349
Silk, J. 2001, MNRAS, 324, 313
Skillman, E. D. 1996 in The Minnesota Lectures on Extragalactic Neutral Hydrogen, ASP Conference Series, Vol. 106, ed. by E. D. Skillman (San Francisco: ASP), 208
Swaters, R. A. 1999, Ph.D. Thesis, University of Groningen
Swaters, R. A., Madore, B. F., & Trewhella, M. 2000, ApJ, 531, L107
Swaters, R. A., Schoenmakers, R. H. M., Sancisi R., & van Albada T.S. 1999, MNRAS, 304, 330
van den Bergh, S. 1995, AJ, 110, 613
van den Bosch, F. C., Burkert, A., & Swaters, R. A. 2001, MNRAS, 326, 1205
van den Bosch, F. C., Robertson, B. E., Dalcanton, J. J., & de Blok, W. J. G. 2000, AJ, 119, 1579
van der Hulst, J. M., Skillman, E. D., Smith, T. R., Bothun, G. D., McGaugh S. S., & de Blok W. J. G. 1993, 106, 548
Windhorst, R. A. et al. 2002, submitted to ApJS
Zaritsky, D. & Rix, H.-W. 1997, ApJ, 477, 118

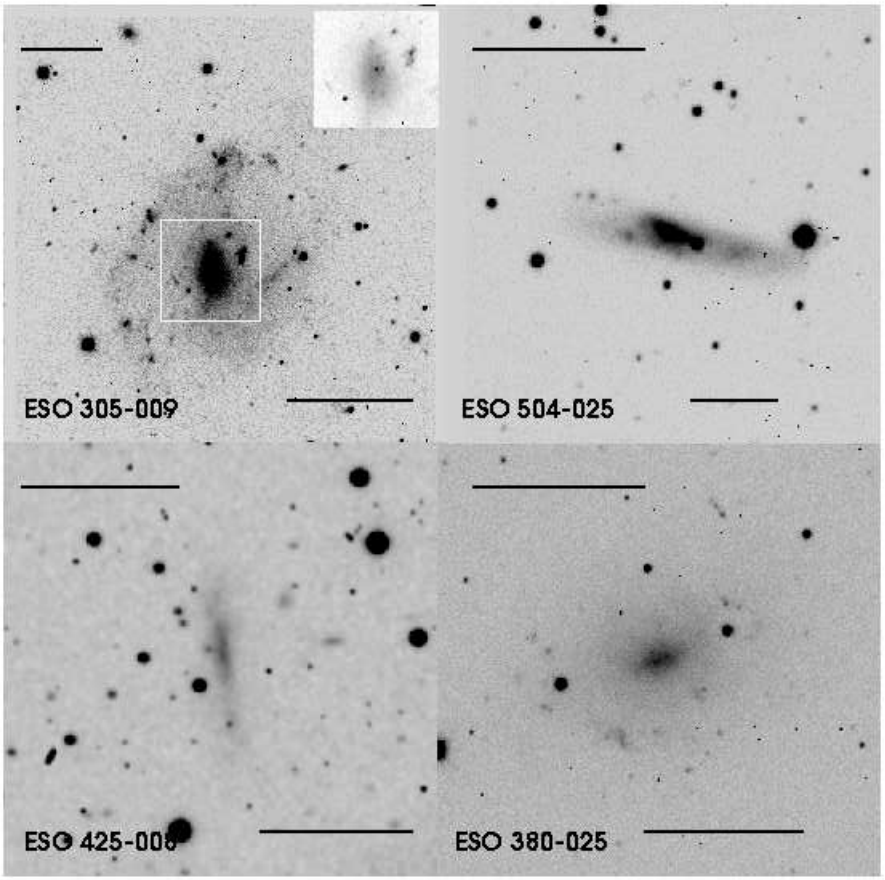

FIG. 1.— Sample V-band CCD images of 4 of our program galaxies: ESO 305-009 (top left), ESO 504-025 (top right), ESO 425-008 (bottom left), and ESO 380-025 (bottom right). The scale bars on each panel indicate 1 arcminute (upper) and 5 kpc at the adopted distance of the galaxy (lower). The inset on the ESO 305-009 panel highlights the pointlike nucleus in this galaxy. Narrow band Hα images as well as our new Hα spectroscopy confirm this feature is not a foreground star (see Section 5.3). ESO 380-025 also has a pointlike nucleus. These imaging data are described in detail in MG97.

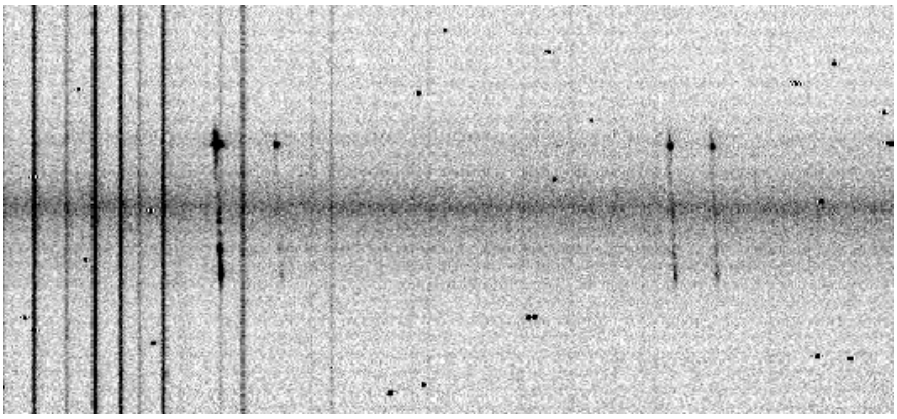

FIG. 2.— Sample longslit spectrum for the galaxy ESO 502-016. The x-axis is the dispersion axis, with λ increasing from left to right, and the y-axis is the spatial axis. The spectrum has been trimmed to show a field-of-view along the spatial axis of $\sim$2′.6. The horizontal band through the center of the image is the galaxy continuum, and the bright vertical lines extending the full height of the image are the telluric OH sky lines. The visible galactic emission features correspond, from left to right, to the redshifted lines of: Hα $\lambda\lambda$6562.82Å [N II] λ6583.41Å and [S II] $\lambda\lambda$6718.26,6732.64Å. The small black specks on the image are due to cosmic rays.

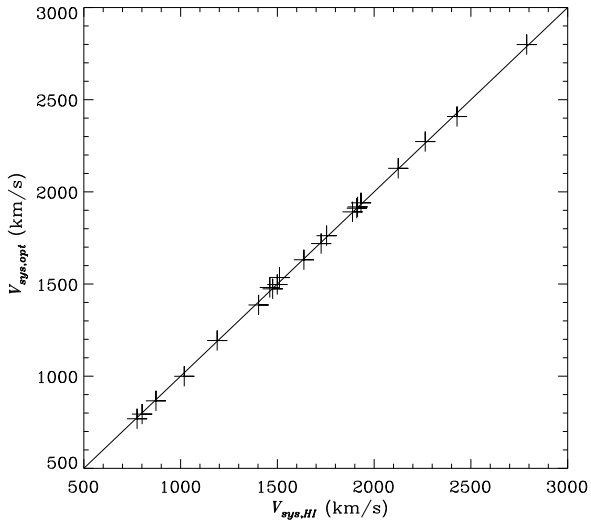

FIG. 3.— Comparison of systemic radial velocities derived from our new Hα spectroscopic observations with those derived from global H I measurements (see also Table 2).

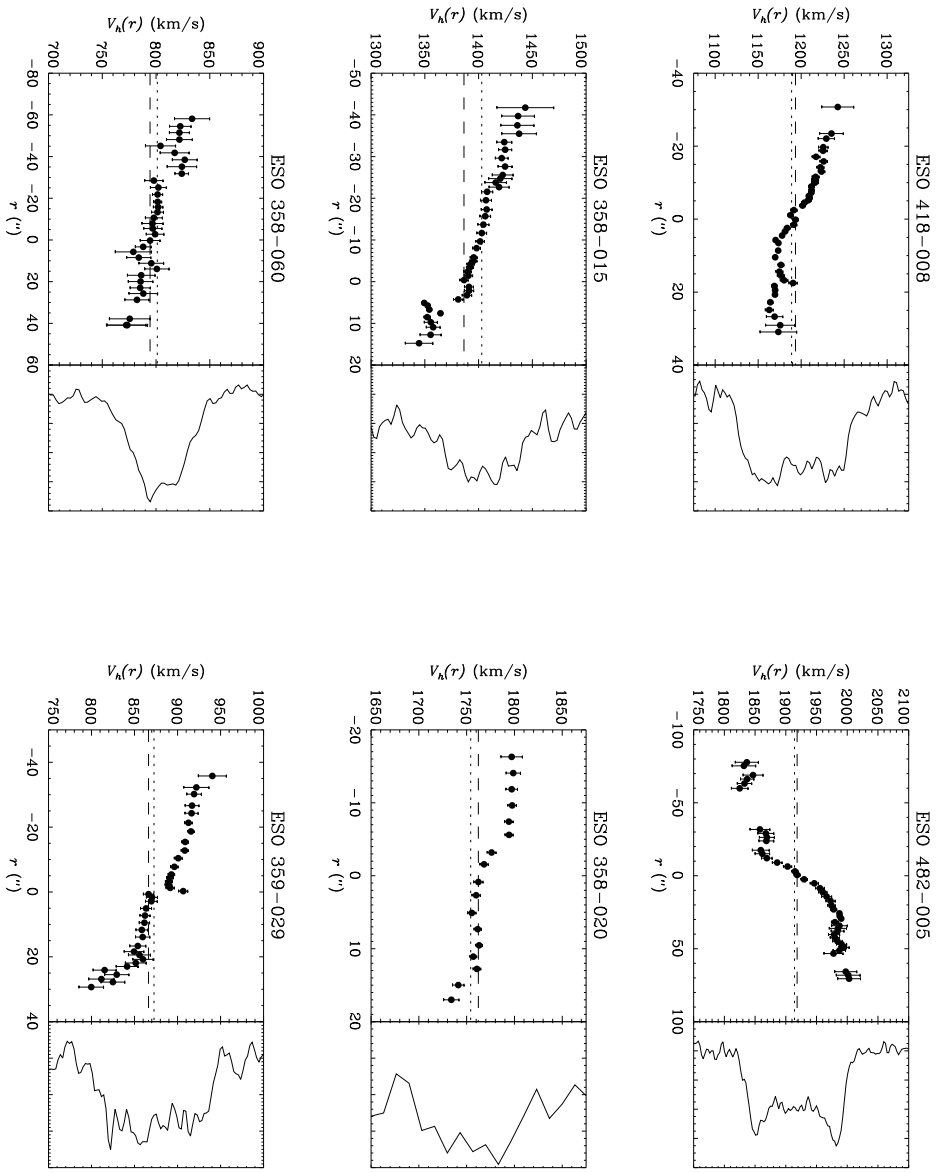

FIG. 4.— Hα position-velocity (P-V) curves for the 21 extreme late-type spirals observed in the present study. Axes are heliocentric radial velocity (in kilometers per second) versus distance from the galaxy center (as defined by the nuclear continuum), in arcseconds. When available, the global H I spectrum of the galaxy from Matthews et al. (1998) is plotted alongside the optical data. The global H I spectra are plotted as heliocentric velocity (on the same scale as the optical data) versus flux density (in arbitary units). The horizontal dashed lines indicate the systemic velocities derived from the optical observations, while the horizontal dotted lines indicate the systemic velocities derived from the global H I observations of Matthews et al. (1998) or Fouqué et al. (1990).

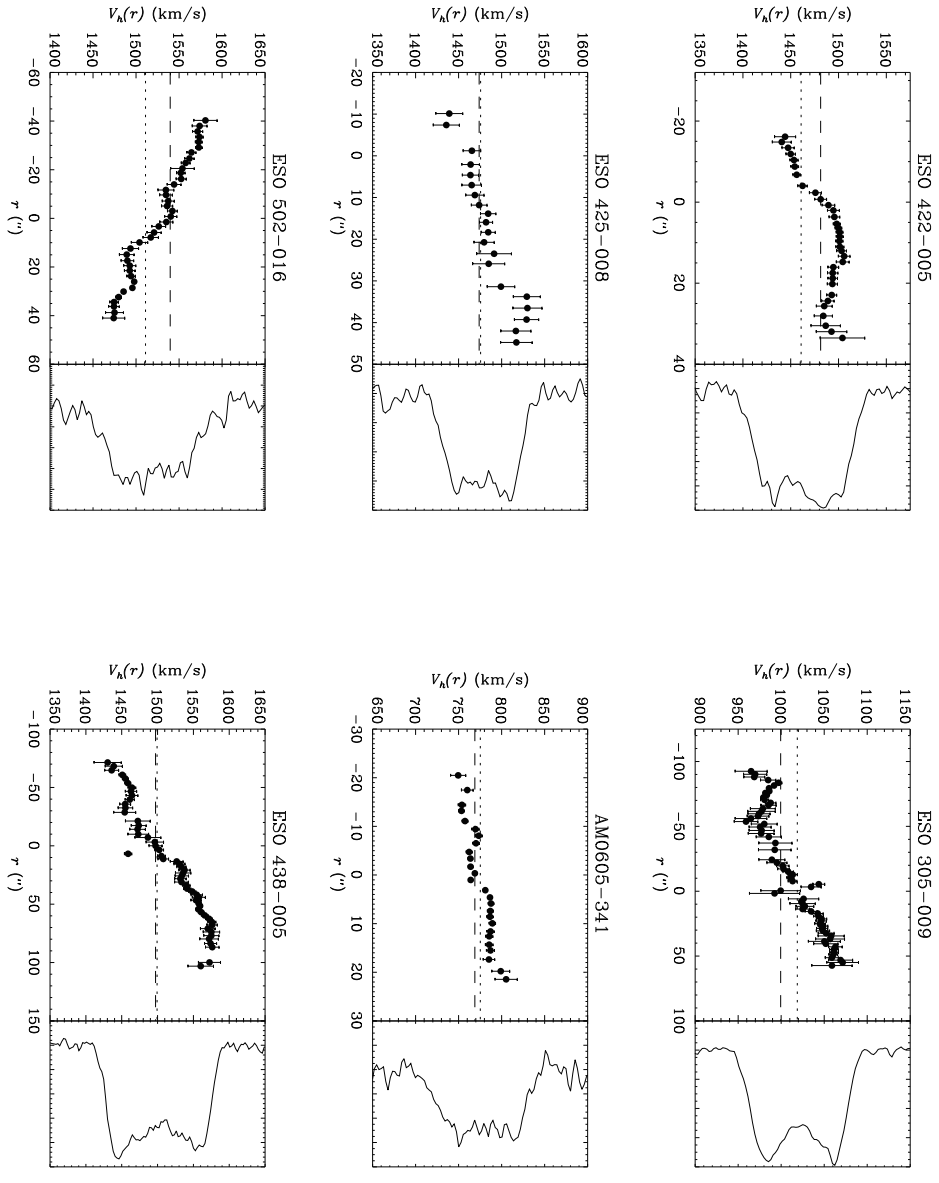
ESO 422−005
ESO 425−008
ESO 502−016
ESO 305−009
AM0605−341
ESO 438−005
$V_h(r)$ (km/s)
r (")

FIG. 4.— cont.

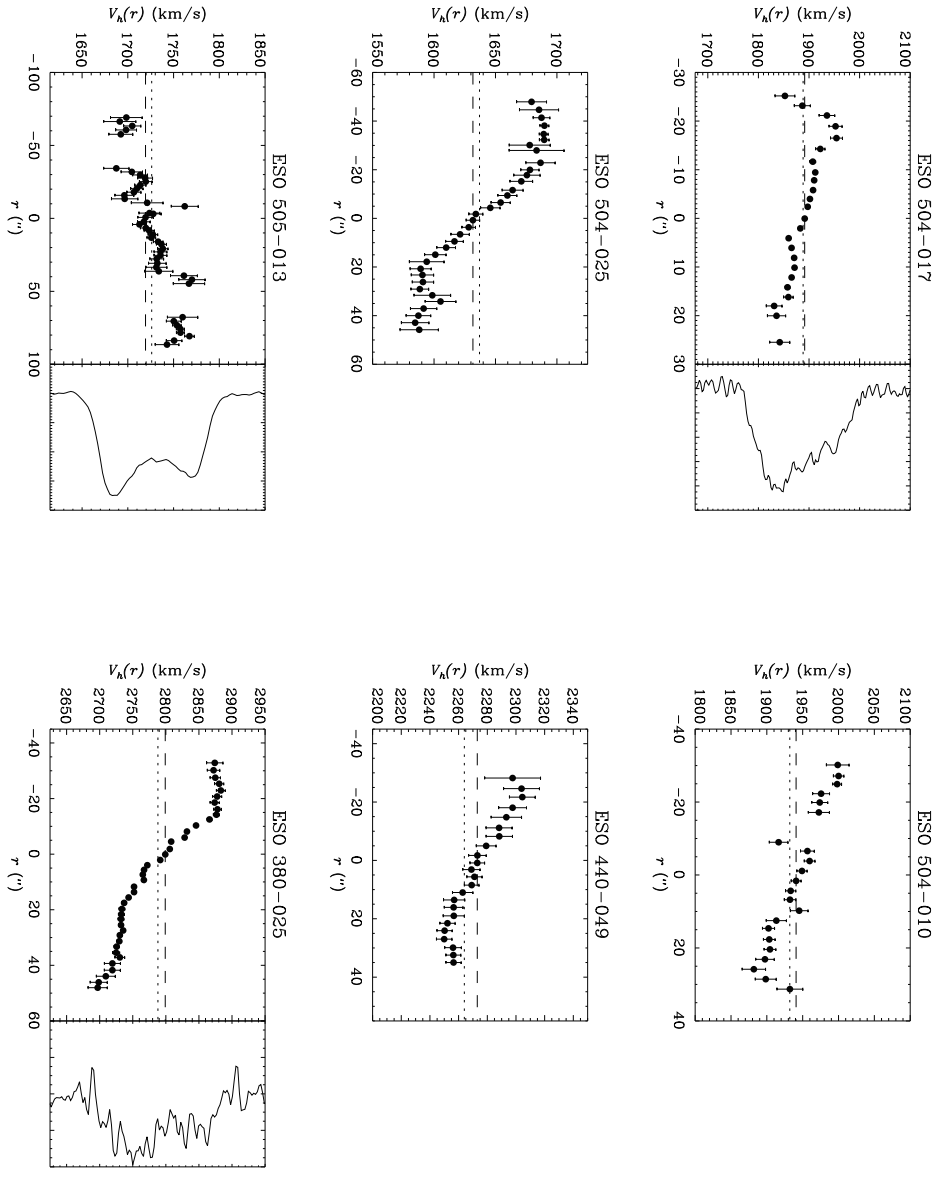
ESO 504−017
ESO 504−025
ESO 505−013
ESO 504−010
ESO 440−049
ESO 380−025
$V_h(r)$ (km/s)
r (")

FIG. 4.— cont.

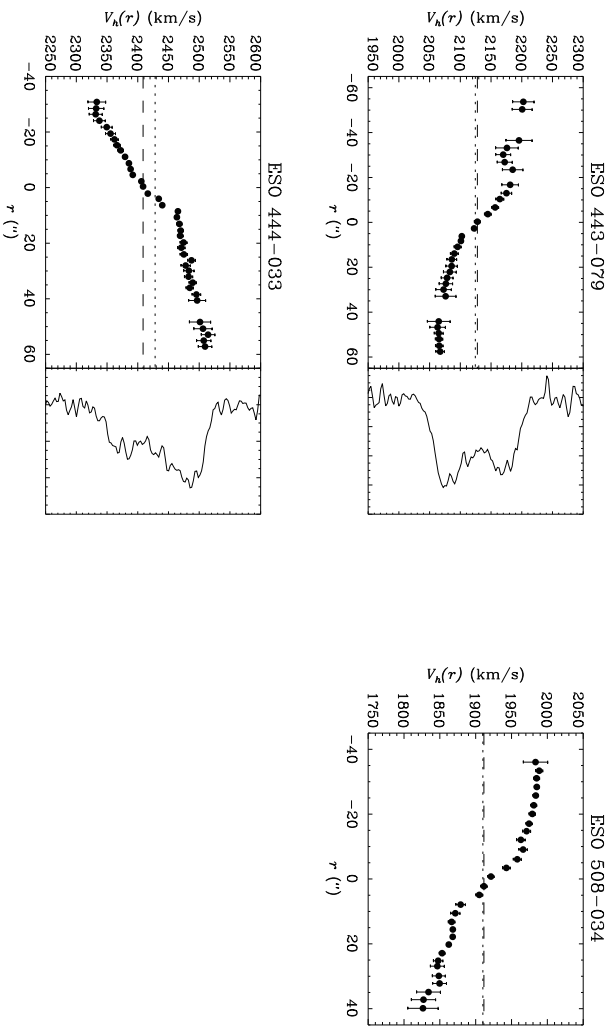

FIG. 4.— cont.

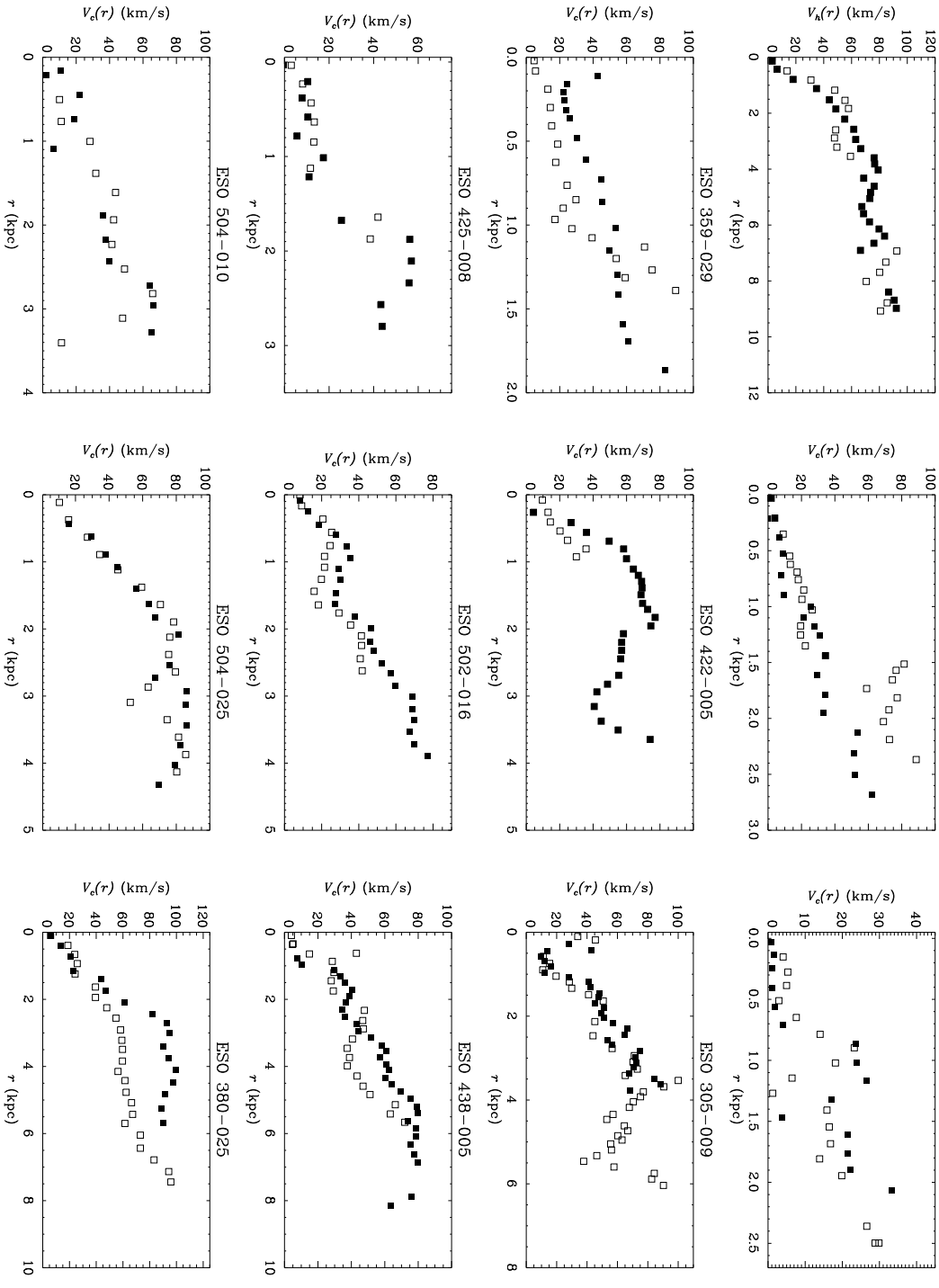

FIG. 5.— Major axis rotation curves for 15 galaxies in our sample. The data are corrected for inclination and offsets between the spectrograph slit and the true disk major axis (see Text for further details). Data points from the approaching side of the galaxy are shown as open symbols and data from the receding side are shown as filled symbols.

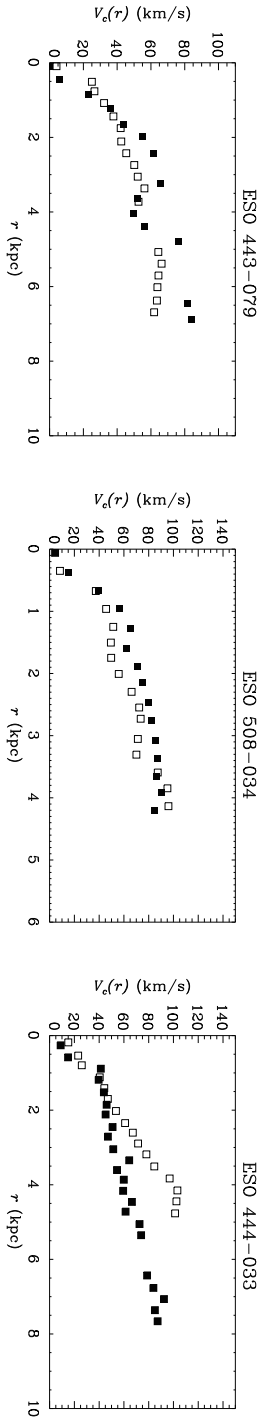

FIG. 5.— cont.

TABLE 1
SUMMARY OF OBSERVATIONS

Galaxy Name	Type	α (1950.0) (^{h} ^{m} ^{s})	δ (1950.0) ($^\circ$ $'$ $''$)	n	t (s)	ϕ_{ma} ($^\circ$)	ϕ_{slit} ($^\circ$)	$\lvert\Delta\phi\rvert$ ($^\circ$)
(1)	(2)	(3)	(4)	(5)	(6)	(7)	(8)	(9)
ESO418-008	SBdm	03 29 28	-30 22 54	2	1500	0	140[1]	40
ESO482-005	SBd	03 30 52	-24 18 06	2	1800	79	80	1
ESO358-015	Sdm	03 31 10	-34 58 30	2	2000	16	180	16
ESO358-020	SBdm	03 32 58	-32 48 18	2	1500	165	167	2
ESO358-060	Sm	03 43 18	-35 43 30	2	2000	102	102	0
ESO359-029	Sdm	04 10 56	-33 07 42	2	2000	20	20	5
ESO422-005	Sdm	04 50 07	-28 40 30	1	1000	35	15	20
ESO305-009	SABc	05 06 26	-38 22 30	2	2000	90	63[1]	27
ESO425-008	SBm:	06 04 38	-27 52 18	2	1800	80	80	0
AM0605-341	SBdm	06 05 31	-34 11 49	1	750	90	90	0
ESO502-016	SBd	11 02 48	-26 21 18	1	1200	82	79	3
ESO438-005	Sd	11 06 33	-28 06 00	2	2000	62	60	2
ESO504-010	SBdm	11 40 32	-23 09 18	1	1200	14	15	1
ESO504-017	Scd/BCD	11 46 15	-27 06 00	1	500	60	103	43[2]
ESO504-025	Sd	11 51 18	-27 04 18	2	1800	30	20	10
ESO440-049	Sc	12 02 59	-31 08 42	2	1800	0	60	60
ESO505-013	SABc	12 03 33	-22 34 18	1	900	135	45	90[2]
ESO380-025	SBdm	12 21 56	-35 07 54	1	1000	15	13	2
ESO443-079	SABd	13 07 38	-27 42 18	2	2000	0	180	0
ESO508-034	Spec	13 14 13	-25 04 24	1	900	132	129	3
ESO444-033	SBdm	13 23 16	-31 52 12	1	1000	89	88	1

[1]Slit was placed along the galaxy's bar.

[2]Major axis position angle is uncertain owing to the small inclination of the disk (see Table 2).

NOTE.—Explanation of columns: (1) galaxy name; (2) Hubble classification from MG97 (3) & (4) right ascension and declination, epoch 1950.0; (5) number of exposures obtained; (6) total exposure time, in seconds; (7) position angle of the disk major axis, in degrees (as measured east from north) from Lauberts & Valentijn 1988 or MG97; (8) position angle of spectrograph slit; (9) misalignment, in degrees, between slit position angle and photometric major axis of galaxy.

TABLE 2
PHOTOMETRIC AND SPECTROSCOPIC PARAMETERS

Galaxy Name	Photom. Props.			H I Props.			Opt. Spec. Props.			Ref.
	D_{26}	M_V	i	W_{20}	W_{50}	V_{HI}	$D_{H\alpha}$	$\Delta V_{H\alpha}$	$V_{h_{opt}}$	
(1)	(2)	(3)	(4)	(5)	(6)	(7)	(8)	(9)	(10)	(11)
ESO418-008	1.91	−17.4	55.0	153.5	125.0	1188.9	0.64	79.6	1193.4	1
ESO482-005	2.60	−17.0	81.3	170.8	153.7	1914.2	1.54	178.1	1918.4	1
ESO358-015	1.53	−16.3	46.7	100.2	67.8	1402.9	0.59	98.8	1386.4	1
ESO358-020	1.93	−17.7	37.1	117.7	98.1	1754.2	0.35	64.8	1762.2	1
ESO358-060	2.24	−14.3	85.1	82.0	54.0	801.2	1.03	61.2	794.4	1
ESO359-029	1.92	−15.8	56.4	141.1	134.2	872.6	0.68	140.8	866.3	1
ESO422-005	1.70	−16.7	41.7	126.2	99.0	1460.9	0.73	65.3	1481.3	1
ESO305-009	4.63	−17.2	52.9	129.8	113.1	1018.8	1.56	112.4	999.4	1
ESO425-008	1.20	−14.1	78.8	106.5	91.3	1475.5	0.57	94.3	1473.9	1
AM0605-341	1.27	−15.4	26.0	124.2	95.3	775.2	0.44	55.8	768.9	1
ESO502-016	2.46	−17.2	67.1	155.0	102.8	1511.0	0.85	106.7	1540.3	1
ESO438-005	3.40	−16.7	80.0	163.9	145.5	1499.4	1.86	145.9	1497.2	1
ESO504-010	1.44	−16.2	67.2	145	127	1932	0.64	118.3	1940.8	2
ESO504-017	1.10	−18.0	30.8	220.1	169.3	1888.3	0.55	123.2	1891.5	1
ESO504-025	2.42	−17.2	39.9	137	118	1637	1.06	105.2	1631.6	2
ESO440-049	2.22	−18.5	32.0	151	131	2264	0.78	54.5	2273.0	2
ESO505-013	2.96	−18.8	18.3	132.2	117.3	1726.1	1.62	82.6	1719.4	1
ESO380-025	1.63	−18.6	76.9	180.6	163.9	2788.1	0.84	186.1	2799.2	1
ESO443-079	2.18	−17.2	72.8	157.7	136.3	2124.4	1.16	132.5	2127.8	1
ESO508-034	1.53	−17.5	64.6	167	150	1910	0.79	162.2	1911.5	2
ESO444-033	2.03	−17.9	74.3	169.0	147.0	2428.2	0.92	182.9	2408.7	1

NOTE.—Photometric parameters are taken from MG97. H I parameters are taken from the references in Column (11). Quantities in Columns (8)-(10) are measured from the data presented in this work. Explanation of columns: (1) galaxy name; (2) optical diameter in arcminutes; (3) absolute V magnitude; (4) disk inclination in degrees; (5) & (6) measured global H I profile width at 20% and 50% peak maximum, respectively, in kilometers per second; (7) heliocentric recessional velocity measured from H I data, in kilometers per second; (8) extent of measured Hα emission, in arcminutes; (9) measured amplitude of the Hα velocity curve, in km s^{-1}, from the minimum on approaching side to the maximum on the receding side of the disk (uncorrected for inclination and slit position angle); (10) heliocentric recessional velocity derived from our new optical measurements (see Section 5.1); (11) reference for quoted H I parameters.

REFERENCES.—(1) Matthews et al. 1998; (2) Fouqué et al. 1990

TABLE 3
POSITION-VELOCITY DATA

Galaxy Name	x ($''$)	$V_c(x)$ (km s^{-1})	$\sigma_V(x)$ (km s^{-1})
(1)	(2)	(3)	(4)
ESO482-005	70.5	2003.0	18.5
	68.1	2001.5	19.4
	65.7	1997.5	17.9
	53.3	1977.6	15.4
	51.2	1987.1	10.1
	49.0	1994.7	8.2
	46.9	1990.7	8.2
	44.8	1984.0	7.8
	42.4	1979.8	7.5
	40.3	1978.5	9.0
	37.8	1984.2	10.4
	36.0	1984.8	14.0
	34.2	1987.3	12.7
	31.8	1979.9	5.6
	29.4	1990.1	3.5
	27.6	1987.6	3.3
	25.7	1987.3	3.3
	23.0	1977.8	5.1
	20.3	1974.2	6.2
	17.2	1972.8	7.5
	14.2	1966.4	8.2
	11.2	1960.1	6.8
	8.5	1955.5	7.1
	5.1	1946.4	6.7
	2.4	1929.8	5.0
	-0.5	1918.4	4.8
	-2.9	1914.9	4.9
	-6.3	1902.8	6.7
	-9.0	1885.9	7.8
	-12.0	1869.0	8.6
	-15.0	1861.7	11.8
	-17.5	1859.2	13.7
	-23.8	1868.3	12.1
	-26.2	1869.2	12.2
	-29.0	1867.5	12.9
	-31.7	1857.8	16.1
	-59.8	1824.9	13.5
	-63.2	1832.7	11.7
	-66.2	1837.1	10.9
	-68.9	1846.7	16.2
	-75.3	1831.8	19.2
	-77.7	1836.5	18.8

NOTE.—Measured Hα position-velocity data for the program galaxy ESO 482-005. The data for the full sample are available in electronic format. Columns are (1) galaxy name; (2) position x along the major axis in arcseconds; (3) heliocentric radial velocity at position x (using the optical convention $V_c(x) = (\lambda - \lambda_0)c\lambda_0^{-1}$, where λ is the measured wavelength of the Hα emission, c is the speed of light, and λ_0 is the rest wavelength of Hα); (4) uncertainty in the radial velocity measurement in km s^{-1}.

APPENDIX

COMMENTS ON INDIVIDUAL SPECTRA

ESO 418-008: The shallow amplitude of the Hα P-V curve relative to the global H I profile likely partially arises from the positioning of the spectrograph slit along the galaxy bar, which is displaced $\sim$40° from the galaxy major axis.

ESO 358-015: The break in this galaxy's P-V curve near V_{sys} appears to correspond to the location of the galaxy's semi-stellar nucleus, which is displaced from the dynamical center of the galaxy as defined by both the global H I profile and the optical continuum emission. The Hα P-V curve is strongly asymmetric, as is the stellar disk of the galaxy. These strong asymmetries suggest that the offset between the measured optical and radio radial velocities may be real, and a consequence of a true offset between the stellar and the H I disks. Near the galaxy's nucleus, the Hα emission lines contain a broad wing on the redward side; some of the Hα emission features near the galaxy nucleus also appear double-peaked.

ESO 358-060: The Hα P-V curve extends significantly farther on the approaching side than on the receding side. This galaxy does not appear to have spiral arm structure or strong internal absorption, hence the "wiggles" in its P-V curve likely result from a very patchy distribution of H II regions.

ESO 359-029: The reversal seen near the center of this rotation curve appears to correspond to the location of this galaxy's semi-stellar nucleus (see also Matthews et al. 1999). Weak asymmetries are seen in both the optical P-V curve and the global H I profile. Possible Hα absorption may be present.

ESO 422-005: It is unlikely that a misalignment of 20° between the spectrograph slit and the disk major axis can account for the discrepancy between the optical and radio V_{sys} values, or the odd shape of the optical P-V curve, which on the receding side shows a rise, then falls to near V_{sys} before once again rising. This galaxy shows an asymmetry in the global H I profile in terms of the shape of the rotation peaks, as well as a weak asymmetry in the stellar disk (see also MG97).

ESO 305-009: Strong nuclear continuum present. A reversal in the optical P-V curve near V_{sys} occurs at the location of this galaxy's semi-stellar nucleus. A misalignment of $\sim$27° between the slit placement and the galaxy major axis may partially account for the odd shape of the rotation curve, which on the approaching side shows a rise, then falls to near V_{sys} before once again rising.

ESO 425-008: The peak of the optical continuum shows a large spatial asymmetry relative to the velocity centroids of both the optical P-V curve and the global H I profile.

AM 0605-341: This galaxy shows very little rotation in its stellar disk. The global H I profile is significantly broader than the amplitude of the Hα P-V curve, indicating this galaxy must have extended H I and reach its maximum rotational velocity well outside of its stellar disk. The Hα lines near the center of this galaxy are rather broad. Our spectra suggest presence of a possible starburst nucleus.

ESO 502-016: The asymmetries in the stellar disk and the global H I profile of this galaxy suggest that the observed offset between the optical and radio V_{sys} values may be real. The galaxy does not show any obvious features in the optical disk to explain the wavy appearance of the P-V curve.

ESO 438-005: A small break occurs in the Hα P-V curve of this galaxy near V_{sys}, which may result from this galaxy's weak bar.

ESO 504-010: The breaks that occur in the Hα P-V curve, slightly offset from V_{sys}, may be caused by this galaxy's bar.

ESO 504-017: The slit was misaligned by $\sim$43° from the galaxy major axis during the observations of this galaxy. However, since the disk has a relatively low inclination ($i \approx$31°), this probably did not affect the observed P-V curve significantly, which shows a very low amplitude in the inner regions of the galaxy. This galaxy was shown by Matthews et al. (1998) to have rather extended H I.

ESO 504-025: The slight "glitch" seen in the optical P-V curve near V_{sys} appears to be due to this galaxy's semi-stellar nucleus. The P-V curve is observed to flatten off, but distinct dips are seen on the flat part of the P-V curve near radii of $\pm 33''$ from the galaxy center.

ESO 440-049: Very strong nuclear continuum present. The bright continuum as well as the slight perturbation seen near V_{sys} may be due to this galaxy's small bulge component.

ESO 505-013: Strong nuclear continuum present. This galaxy contains spiral arms clearly delineated by H II regions, as well as a semi-stellar nucleus. The ripples in the optical P-V curve may be due to the spiral arm pattern, while the rotation curve reversal seen near V_{sys} is likely due to the semi-stellar nucleus. The rotation curve is spatially more extended on the receding side, while the global H I profile contains slightly more flux on the approaching side. The slit was placed near the galaxy's minor axis during these observations, but because of the galaxy's small inclination ($i \approx 18°$), the observed shape of the P-V curve was probably not significantly affected.

ESO 380-025: The shape of the Hα P-V curve shows significant differences on the receding and approaching sides, with the receding side flattening off, and the approaching side continuing to rise to the last measured point.

ESO 443-079: The Hα P-V curve appears to flatten near 2.2 radial scale lengths. Both the approaching and receding sides show a break near at roughly $\pm 40''$ from the galaxy center.

ESO 444-033: Both the approaching and receding sides of the Hα P-V curve are quite linear in shape, but have differing slopes. The V_{sys} value measured from the global H I spectrum appears to better correspond to the rotation curve center

than the optically-derived value. Both the optical galaxy and the global H I profile are very asymmetric, thus the observed offset between the optical and radio V_{sys} values may be real.

This figure "MatthewsL_fig1.png" is available in "png" format from:

http://arXiv.org/ps/astro-ph/0203188v1